might be imperfect. The wavefront should be overlapped completely. The walk-off in the nonlinear crystal and window material causes the beam displacement of around 0.1 mm. A wedge plate which can change the direction of the beam axis may reduce the baseline variations. Similar to that, the distortion of the wavefronts, which is due to multi-reflection in the window material or the PEM, also causes the imperfections of vibration cancellation. One of the solutions is an adaptive optics, which consists of a wavefront sensor and a deformable mirror. As for long time measurement, observed slow variations are speculated to be related to changes in the room temperature. The temperature variations might change the optical constant of some optical components.

The electron density of an atmospheric-pressure plasma, whose density response is almost the same (within several μs) as that of the discharge current was conducted, in order to evaluate the actual temporal response of the DI. The plasma source was placed just in front of the PEM and the laser beam is focused on the micro plasma[16] by adding lenses. From the measurements, it is found that there is a delay time of about 80 μs in the evaluated density compared with the actual density rise. The time constant of the evaluated density is about 100 μs in the case of a time constant of the lock-in amplifier of 30 μs. These characteristics of the responses are expected to come from the lock-in amplifiers. The digital lock-in technique, which has been adopted in the MSE,[17] would improve the time response of the DI.

Measurement results of LHD plasma with the DI and the existing far infrared laser interferometer are shown in Figs. 6(a) and 6(b). Although the lines of sight are different from each other (FIR: vertical line of sight, DI: horizontal line of sight), they show good agreement. One of the possible reasons for the about 5% averaged difference between the DI and the far infrared laser interferometer, shown in Fig. 6(c), is an error of the optical path length in a plasma. The optical path lengths are defined as the distance inside the last closed magnetic surface (LCFS) which is determined by equilibrium calculations. However, the density of the LHD plasma actually expands to the stochastic layer outside the LCFS and the expansion is different at each cross section. The modulation of the evaluated density with the DI $\Delta n_e = n_e^{Dis} - 0.96 \times n_e^{FIR}$ of an amplitude of $\pm 2 \times 10^{18}$ m^{-3}, is seen as shown in Fig. 6(c). This modulation is caused by offsets included in the amplitudes of the modulation I_{ω_m}, $I_{2\omega_m}$ for the density evaluation. Supposing that the offsets C and D are added to the amplitude signals,

$$I_{2\omega_m} = 2BJ_2(2\rho_0)\cos(\psi) + C,$$
$$I_{\omega_m} = -2BJ_1(2\rho_0)\sin(\psi) + D.$$

Then the additional modulation term appears in the evaluated phase shift ψ':

$$\psi' = \tan^{-1}(I_{\omega_m} / I_{2\omega_m}) = -\psi + E\sin(c\psi + \alpha). \quad (6)$$

The offset, which was about 10% of the modulation amplitudes, was found in the amplitude signals. Supposing that

$$C/2BJ_2(2\rho_0) = D/2BJ_1(2\rho_0) = 0.1, \quad (7)$$

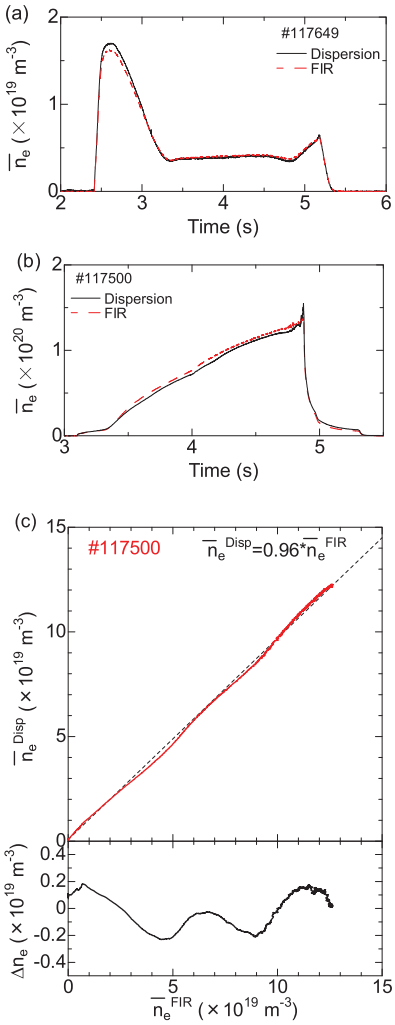

FIG. 6. (a) and (b) Measurement results of low and high density plasmas with the dispersion interferometer n_e^{Dis} and with the far infrared laser interferometer n_e^{FIR}. (c) Comparison between n_e^{Dis} and n_e^{FIR}. An oscillation of the electron density $\Delta n_e = n_e^{Dis} - 0.96 \times n_e^{FIR}$ is found.

the expected density modulation calculated with Eq. (6) is $\pm 1 \times 10^{18}$ m^{-3}, which is close to the measurement results. One of the possible reasons of the offset in the modulation amplitudes is the multi-reflection inside the optical element in the PEM. The multi-reflected lights interfere with each other and the amplitudes of the interference signal will be modulated with the harmonics of the drive frequencies due to slight changes in the thickness of the optical element or change in the refractivity. In order to reduce the offsets, optimization of the incident angle of the laser beam to the PEM to minimize the multi-reflections may be effective.

The fringe jump errors occur easily in the high density range because of fast density change or beam refraction in a plasma. Since there is no density limit such as the Greenwald density in tokamaks, the high density larger than 1×10^{20} m^{-3}, which is comparable to that in ITER standard operation, can be available on LHD. Hence, LHD is a good test platform for robust density measurements. Figure 7 shows measurement results of the high density discharge up to 1.5×10^{20} m^{-3} sustained by repetitive pellets injection. While a fringe jump error occurred in the

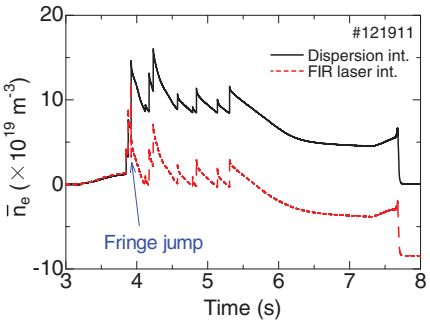

FIG. 7. The temporal evolutions of the line averaged electron density measured with the dispersion interferometer and the far infrared laser interferometer. The fringe jump error occurs at $t = 3.92$ s, as shown by an arrow.

far infrared laser interferometer due to decrease in the detected intensity by beam refraction, the DI can continue measurement. The decrease in the detected intensity was not significant due to shorter wavelength and the DI could track a fast density change of 7.8×10^{20} m^{-3}, which corresponds to 1.8 fringe, during 1 ms by a sampling rate of 100 kHz and with a time constant of lock-in amplifier of 30 μs.

V. DISCUSSION

To be free from fringe jump errors, the expected phase shift should be smaller than 2π. Although there were no fringe jump errors in the pellet injected discharge by the sufficient sampling frequency and the time constant, there still remains the risk of fringe jump errors for the CO_2 laser DI principally because the phase shift is larger than one fringe. A Nd:YAG laser, whose wavelength is 1.064 μm can reduce the phase shift down to 1/10 compared with that of the CO_2 laser. The line density which corresponds to 2π is 1.4×10^{21} m^{-2} for Nd:YAG laser. In case of LHD (optical path length is 3.28 m in double path), even 3×10^{20} m^{-3} which is the maximum line averaged electron density so far, the phase shift is 0.58 fringe and the density can be determined without ambiguity of 2π.

The Nd:YAG laser DI can be composed of commercial optical components. There is a continuous wave Nd:YAG laser with a power of more than 1 W. There are varieties of nonlinear crystals and PPMgSLT has a high conversion efficiency. Combined with the above laser whose output power is 8 W, the second harmonic beam with a power of 2 W will be obtained with PPMgSLT. A high sensitivity detector for the second harmonics is available and about 1 mW is enough for detection. However, 1 μm laser beam is easily attenuated by the surface roughness of the in-vessel mirrors, which is caused by sputtering and depositions of impurities. The reflectivity at the visible light decreased down to less than 10%[18] on LHD, two-three orders higher power is preferable. As for the phase modulator, not only the PEM but also an electro-optic modulator (EOM) is available in this wavelength range, whose drive frequency is higher (e.g., 1 MHz) than that for the PEM. Hence, a faster time response can be expected. One of the concerns is the smaller signal to noise ratio (SNR). This is because the phase shift due to a plasma becomes one order smaller and that due to the vibrations becomes one order larger. In addition to that, the wavefront distortion would be more serious than that for the CO_2 laser. The bench-testing for the examination of SNR of the Nd:YAG laser DI is proceeding in NIFS at present.

VI. SUMMARY

A CO_2 laser (10.6 μm) DI which uses a ratio of modulation amplitudes for phase extraction has been developed on LHD. The DI can improve a limitation of an interferometer: measurement errors due to mechanical vibrations. The original DI suffers from the variations of the detected intensities. The proposed phase extraction method which uses the ratio of modulation amplitudes makes the DI free from the variations of the detected intensities. Hence, the developing DI on LHD is robust against both the mechanical vibrations and the intensity variations.

The phase variations of the DI on LHD are within $\pm 2 \times 10^{17}$ m^{-3} for 3 s without a vibration isolation system on the optical bench. The drift of the baseline is about 5×10^{17} m^{-3} for 30 min. The measurement results of the DI show good agreement with the existing far infrared laser interferometer. The average difference between them of about 5% might come from the evaluation error of the optical path length. The fake density modulation with an amplitude of $\pm 2 \times 10^{18}$ m^{-3} was found during the density ramp-up. The density modulation seems to be attributed to offsets in the amplitudes of modulation components, which are used for the phase evaluations. Since the multi-reflections inside the phase modulator are one of the candidates for what causes the offset, fine adjustment of the incident angle of the probe beam to the modulator would improve the density modulation. In the case of the sufficient sampling rate and time constant of the lock-in amplifiers for amplitude detection of the modulation signal, there is no fringe jump error even in the high density plasma around 1.5×10^{20} m^{-3} sustained by repetitive pellet injections.

For future robust density measurement, a shorter wavelength DI, which adopts a Nd:YAG laser (1.064 μm), can be free from the fringe jump error. The system will be composed by commercial components. The bench-testing for evaluations of signal to noise ratio of the Nd:YAG laser DI which uses the above phase extraction method is in operation.

[1] Y. Kawano, S. Chiba, and A. Inoue, Rev. Sci. Instrum. **72**, 1068 (2001).
[2] H. K. Park, C. W. Domier, W. R. Geck, and N. C. Luhmann, Jr., Rev. Sci. Instrum. **70**, 710 (1999).
[3] T. Akiyama, S. Tsuji-Iio, R. Shimada, K. Nakayama, S. Okajima, M. Takahashi, K. Terai, K. Tanaka, T. Tokuzawa, and K. Kawahata, Rev. Sci. Instrum. **74**, 2695 (2003)
[4] Ch. Fuchs and H. J. Hartfuss, Phys. Rev. Lett. **81**, 1626 (1998).
[5] T. Akiyama, K. Kawahata, Y. Ito, S. Okajima, K. Nakayama, S. Okamura, K. Matsuoka, M. Isobe, S. Nishimura, C. Suzuki *et al.*, Rev. Sci. Instrum. **77**, 10F118 (2006).
[6] F. A. Hopf, A. Tomita, and G. Al-Jumaily, Opt. Lett. **5**, 386 (1980).
[7] Kh. P. Alum, Yu. V. Koval'chuk, and G. V. Ostrovskaya, Sov. Tech. Phys. Lett. **7**, 581 (1981).
[8] V. P. Drachev, Yu. I. Krasnikov, and P. A. Bagryansky, Rev. Sci. Instrum. **64**, 1010 (1993).
[9] P. A. Bagryansky, A. D. Khilchenko, A. N. Kvashnin *et al.*, Rev. Sci. Instrum. **77**, 053501 (2006).
[10] F. Brandi and F. Giammanco, Opt. Lett. **32**, 2327 (2007).

[11]A. Lizunov, P. Bagryansky, A. Khilchenko *et al.*, Rev. Sci. Instrum. **79**, 10E708 (2008).
[12]T. Akiyama, K. Kawahata, S. Okajima, and K. Nakayama, Plasma Fusion Res. **5**, S1041 (2010).
[13]T. Akiyama, K. Kawahata, R. Yasuhara, S. Okajima, and K. Nakayama, J. Instrum. **7**, C01055 (2012).
[14]P. Kornejew, H. Dreier, A. Solomakhin, and M. Hirsch, in *Proceedings if the 39th EPS Conference on Plasma Physics*, Stockholm, 2012, p. P5037, available online at ocs.ciemat.es/epsicpp2012pap/pdf/P5.037.pdf.
[15]D. J. Bamford, E. A. Cummings, D. Panasenko, D. B. Fenner, J. M. Hensley, R. L. Boivin, T. N. Carlstrom, and M. A. Van Zeeland, Rev. Sci. Instrum. **84**, 093502 (2013).
[16]K. Urabe, T. Akiyama, and K. Terashima, J. Phys. D **47**, 262001 (2014).
[17]Y. Shi, Rev. Sci. Instrum. **77**, 036111 (2006).
[18]T. Akiyama, K. Kawahata, N. Ashikawa, M. Tokitani, S. Okajima, K. Nakayama, N. Yoshida, A. Ebihara, K. Tokunaga, Y. Ohtawa, and S. Tsuji-Iio, Rev. Sci. Instrum. **78**, 103501 (2007).

Electron kinetic effects on interferometry, polarimetry and Thomson scattering measurements in burning plasmas (invited)[a)]

V. V. Mirnov,[1] D. L. Brower,[2] D. J. Den Hartog,[1] W. X. Ding,[2] J. Duff,[1] and E. Parke[1]
[1]*Physics Department, University of Wisconsin - Madison and the Center for Magnetic Self-Organization in Laboratory and Astrophysical Plasmas, Madison, Wisconsin 53706, USA*
[2]*Department of Physics and Astronomy, University of California Los Angeles, Los Angeles, California 90095, USA*

(Presented 2 June 2014; received 29 May 2014; accepted 12 July 2014; published online 5 August 2014)

At anticipated high electron temperatures in ITER, the effects of electron thermal motion on Thomson scattering (TS), toroidal interferometer/polarimeter (TIP), and poloidal polarimeter (PoPola) diagnostics will be significant and must be accurately treated. The precision of the previous lowest order linear in $\tau = T_e/m_e c^2$ model may be insufficient; we present a more precise model with τ^2-order corrections to satisfy the high accuracy required for ITER TIP and PoPola diagnostics. The linear model is extended from Maxwellian to a more general class of anisotropic electron distributions that allows us to take into account distortions caused by equilibrium current, ECRH, and RF current drive effects. The classical problem of the degree of polarization of incoherent Thomson scattered radiation is solved analytically exactly without any approximations for the full range of incident polarizations, scattering angles, and electron thermal motion from non-relativistic to ultra-relativistic. The results are discussed in the context of the possible use of the polarization properties of Thomson scattered light as a method of T_e measurement relevant to ITER operational scenarios. © *2014 AIP Publishing LLC*. [http://dx.doi.org/10.1063/1.4891176]

I. INTRODUCTION

Toroidal interferometry/polarimetry (TIP), poloidal polarimetry (PoPola), and Thomson scattering (TS) are major optical diagnostics being designed and developed for ITER. Since they are needed for basic machine operation as well as physics studies, accurate measurements are required to meet ITER operational goals. Fundamentally, each of these diagnostics relies upon a sophisticated quantitative understanding of the electron response to laser light propagating through a burning plasma. Improvements in this understanding are being used to guide and constrain the design of these diagnostics, and, once they are operational, will be used to improve measurement accuracy. These improvements will enable proper application of diagnostic measurements to direct real-time feedback control of ITER device operation. The primary focus of our work is to examine the effects of electron thermal motion on the refractive indices and polarization of high-frequency electromagnetic waves (specifically laser light, both directed and scattered).

The magnetized plasma exhibits birefringence, and two orthogonal states of wave polarization with different refractive indices are present. Important consequences of plasma birefringence are the Faraday (FR) effect of rotation of the polarization plane and the Cotton-Mouton effect (CM) leading to both rotation and deformation of the polarization ellipse.[1] For the waves propagating in the direction of the incident laser beam and used for the purposes of interferometry and polarimetry (I/P), we calculate electron thermal corrections to the interferometric phase and polarization state of the light (FR and CM polarimetry). Our initial results[2] were obtained from a linear in $\tau = T_e/m_e c^2 \ll 1$ isotropic electron temperature model. They have already been included in the error analysis and design projections of the ITER TIP and PoPola systems.[3,4] The new findings are: (1) the precision of the lowest order linear in τ model may be insufficient; we present a more precise model with τ^2-order corrections to satisfy the high accuracy required for ITER TIP and PoPola diagnostics and (2) the linear model is extended from Maxwellian to a more general class of anisotropic electron distributions. This allows us to take into account a shift of distribution due to mean parallel electron drift velocity (current) and effects of temperature anisotropy caused by ECRH or RF current drive systems. The shift mechanism is discussed in relation to the possibility of Fizeau interferometry/polarimetry to measure the equilibrium plasma current density.

Interaction of the laser beam with plasma causes light to scatter away from the direction of the incident light. This low intensity Thomson scattered light is used for electron temperature and density measurements. In application to this diagnostic, we calculate the degree of polarization of incoherent Thomson scattered laser light analytically exactly without any approximations for the full range of incident polarizations, scattering angles, and electron thermal motion from non-relativistic to ultra-relativistic. The results are discussed in the context of the proposal[5] to use the polarization properties of Thomson scattered light as a method of T_e measurement relevant to ITER operational scenarios. The purpose of this paper is to review recent theoretical results in support of optical diagnostics in burning plasmas. The progress achieved

[a)]Invited paper, published as part of the Proceedings of the 20th Topical Conference on High-Temperature Plasma Diagnostics, Atlanta, Georgia, USA, June 2014.

in Thomson scattering analysis will be described first below, followed by interferometry and polarimetry.

II. THOMSON SCATTERING

Incoherent Thomson scattering is routinely used for electron temperature measurement, with T_e proportional to the width of the scattered spectrum.[6] The scattering process changes the polarization of the light, an effect that becomes large in high-temperature burning plasmas and is typically described by the relativistic depolarization factor q (see Ref. 6). This factor quantifies the reduction of scattered spectral intensity caused by relativistic terms $\propto v_e^2/c^2$ in the polarization part of the scattering operator. Although the reduction is referred to as depolarization, it is different from the common understanding of depolarization considered in our paper. Indeed, the aforementioned reduction of intensity takes place even for scattering on a single moving electron. In this case, the scattered electromagnetic wave has a Doppler-shifted frequency but still remains monochromatic and completely polarized. We analyze the superposition effect caused by a large number of randomly moving electrons. It results in broadening of the frequency spectrum and renders the scattered radiation partially polarized even though the incident light is fully polarized.

The loss of polarization is quantified by the *degree of polarization* P, or equivalently by the *degree of depolarization* $D = 1 - P$. The possibility of determining the plasma electron temperature by measuring the degree of depolarization was suggested in Ref. 5. If the degree of polarization dependence on electron temperature is accurately known from theory, the accuracy of such a diagnostic could potentially exceed that of the conventional spectrum-based TS method. Thus motivated, we revisited this topic to analyze whether polarization effects may be suitable for application to advanced TS diagnostics on ITER. In our analysis, we follow Ref. 7, with some important corrections and improvements. In particular, the finite transit time effect[8] is properly incorporated into the scattering operator. Another important improvement is optimal choice of the reference frame for averaging over velocity space. This allows derivation of an exact relativistic analytical expression for the degree of depolarization.[9]

Polarization properties of a non-monochromatic plane wave are characterized by the complex coherency matrix $\mathbf{J}$. The matrix is constructed from time averaged quadratic combinations of the field components and represented, in general, by four real quantities which can be equivalently expressed by four Stokes parameters or 4-component Stokes vector $\mathbf{S}$

$$\mathbf{J} = \begin{pmatrix} \overline{E_x E_x^\star} & \overline{E_x E_y^\star} \\ \overline{E_y E_x^\star} & \overline{E_y E_y^\star} \end{pmatrix} = \frac{1}{2} \begin{pmatrix} S_0 + S_1 & S_2 + iS_3 \\ S_2 - iS_3 & S_0 - S_1 \end{pmatrix}.$$

The S_0 component corresponds to the total intensity of the wave and the remaining components describe the polarization properties. For a purely monochromatic, fully polarized incident wave, the amplitudes and the phases of E_x and E_y are independent of time. In this case $\det|\mathbf{J}| = 0$, leading to the relationship $S_0^2 = S_1^2 + S_2^2 + S_3^2$. Correspondingly, the state of polarization of the incident laser light in TS experiments and the waves used for I/P measurements are described by the reduced three-component unit Stokes vector $\mathbf{s}_i = S_i/S_0 (i = 1, 2, 3)$. The vector $\mathbf{s}$ is characterized by the azimuth (orientation angle) of the polarization ellipse $0 \le \psi < \pi$ (measured from the perpendicular to the scattering plane) and the ellipticity angle $\chi = \pm \arctan(b_2/b_1)$ determined by the ratio of the minor and the major axis ($-\pi/4 < \chi \le \pi/4$). Then, the four-component Stokes vector of fully polarized incident laser light is expressed as $\mathbf{S}^{(i)} = S_0(1, \cos 2\psi \cos 2\chi, \sin 2\psi \cos 2\chi, \sin 2\chi)$.

A fully unpolarized wave (natural light) is characterized by $S_1 = S_2 = S_3 = 0$. Any partially polarized wave can be decomposed into completely unpolarized and polarized portions yielding the degrees of polarization/depolarization of the scattered radiation[10]

$$P = \frac{I_{pol}}{I_{tot}} = \frac{\sqrt{S_1^{(s)2} + S_2^{(s)2} + S_3^{(s)2}}}{S_0^{(s)}}, D = 1 - P.$$

Making use of the definition of the Stokes vector allows us to obtain the 4×4 Mueller matrix that describes the transformation of the Stokes vectors in the process of scattering on a single electron moving with an arbitrary velocity $\mathbf{v}$, $\mathbf{S}^{(s)} = \mathbf{M}^{(single)}(\mathbf{v}) \cdot \mathbf{S}^{(i)}$. Time averaging is performed by integrating over the whole frequency range that removes a delta-function dependence on frequency in $\mathbf{M}^{(single)}$. This corresponds to the transition from the spectrum-based characteristics to the polarization analysis based on the total frequency integrated intensities. As the scattering is incoherent, the Stokes vector of the total scattered radiation is the sum of the Stokes vectors of radiation scattered by the separate electrons. The resulting effect is described by the Mueller matrix $\mathbf{M}(\mu, \theta) = C\mathbf{m}(\mu, \theta)$ averaged over a relativistic Maxwellian distribution

$$m_{00} = 1 + u^2 - 2G(\mu)(u^2 + 4u - 3) + (16/\mu^2)(1 - u)^2,$$
$$m_{01} = m_{10} = 1 - u^2,$$
$$m_{11} = 1 + u^2 + 2G(\mu)(u^2 - 4u + 1) + (12/\mu^2)(1 - u)^2,$$
$$m_{22} = 2u - 4G(\mu)(u^2 - u + 1) - (12/\mu^2)(1 - u)^2,$$
$$m_{33} = 2u - 4G(\mu)u(2u - 1) - (8/\mu^2)(1 - u)^2,$$

while the constant factor $C = r_0^2 N/2r^2$, where r_0, r and N are the classical electron radius, the distance from the scattering volume to the point of observation (detector) and the total number of electrons inside the scattering volume, respectively (see definition of the dimensionless factor N in Sec. II D of Ref. 8). This large factor is important for the intensity of Thomson scattered radiation, but not included in Ref. 7. All integrations in $\mathbf{m}$ are performed in analytical form yielding functions of the scattering angle, $u = \cos\theta$, and electron temperature via the factor $\mu = m_e c^2/T_e$ and function $G(\mu) = K_1(\mu)/(\mu K_2(\mu))$, where K_1 and K_2 are modified Bessel functions of the second kind. These matrix elements present an exact analytical solution for the state of polarization of incoherent Thomson scattering radiation. They are different from Ref. 7 where only the lowest order in τ analytical results were obtained without the finite residence time effect taken into account (the incorrect weighting factor $(1 - \beta_s)^{-6}$ instead of $(1 - \beta_s)^{-5}$).

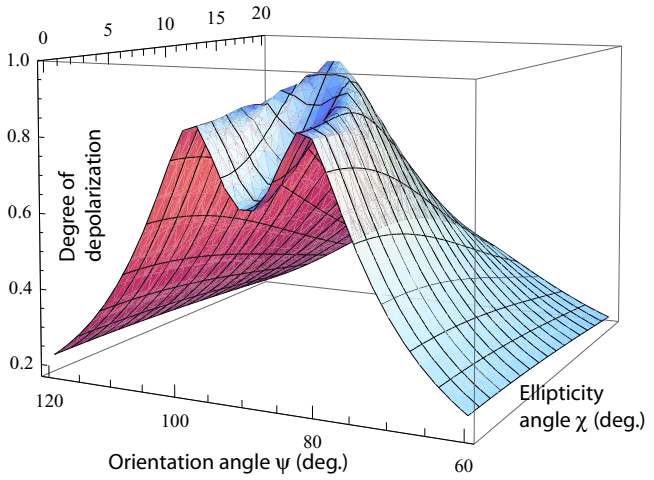

FIG. 1. Depolarization degree vs orientation and ellipticity angles ψ and χ at $\theta = 90^\circ$, $T_e = 10$ keV. There is a local maximum of D at $\psi \simeq 82^\circ$ and $\chi = 0$ (linear polarization), but the absolute maximum is reached at $\psi = 90^\circ$ and $\chi \simeq 9^\circ$ (elliptical polarization). D is an even function of cos ψ illustrated in this figure by plotting $\psi > 90^\circ$.

The degree of depolarization depends on T_e, scattering angle θ, and polarization characteristics of the incident light ψ and χ. One particular example illustrating a maxima of D as a function of ψ and χ is shown in Fig. 1 for $T_e = 10$ keV and $\theta = 90^\circ$. At any given θ and T_e, extrema of D as a function of ψ and χ are reached at the boundaries of the region $0 \le \psi \le \pi/2$, $0 \le \chi \le \pi/4$. This allows us to find the absolute maximum $D_{max}(T_e, \theta)$, and minimum $D_{min}(T_e, \theta)$, with respect to all possible polarization states of the incident radiation, and to set upper and lower limits on D at given θ and T_e. Quantitative pictures of the dependences of these two functions on T_e and θ are shown in Figs. 2 and 3. A good test of correctness

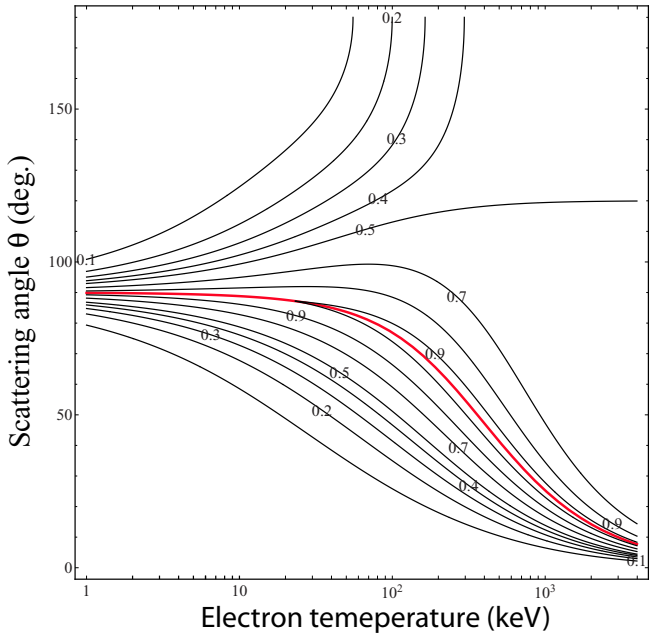

FIG. 2. Contour lines of the maximum value of the degree of depolarization $D_{max}(T_e, \theta)$ (maximized with respect to all possible polarization states of the incident light). The red curve is a boundary in (T_e, θ) space that determines which of the two maxima shown in Fig. 1 provides the absolute maximum.

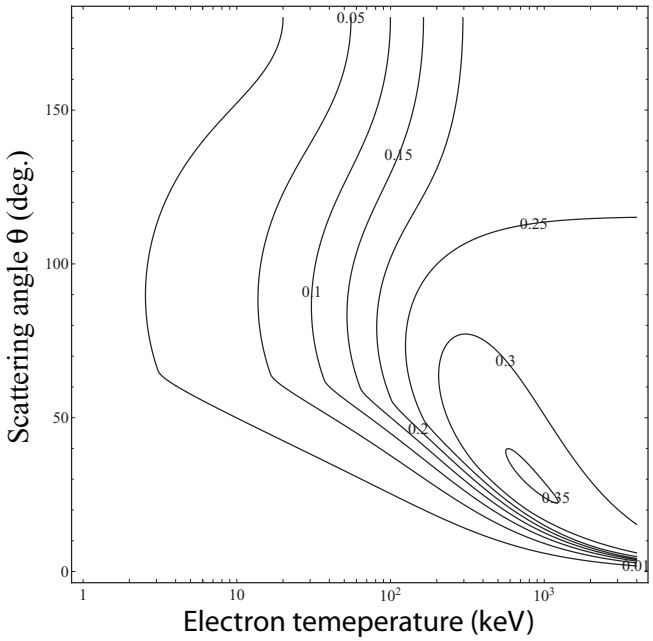

FIG. 3. Contour lines of the minimum value of the degree of depolarization $D_{min}(T_e, \theta)$ (minimized with respect to all possible polarization states of the incident laser light).

of the matrix elements **m** is that for all values of the variables $0 \le D < 1$.

The planned ITER LIDAR TS system detects backscattered radiation at $\theta \sim 180^\circ$. For such backscattered light, the degree of depolarization is quadratic in $\tau \ll 1$ and, therefore, small ($\sim$3% $-$ 5%) at the temperatures expected in ITER. It is insensitive to ψ and reaches its maximum for circularly polarized incident light.[9] For a conventional Thomson scattering geometry with scattering angle $\theta \simeq 90^\circ$, the degree of depolarization of circular polarized incident light is about five times larger ($\sim$20% $-$ 25%). The absolute maximum D_{max} $\sim$ 95% is reached at $\psi = 90^\circ$ for elliptically polarized incident light (see Fig. 1). This extreme regime corresponds to very small scattered power and results in large error bars for polarization-based T_e measurements. More practical cases of circular and linear incident polarizations are illustrated in Fig. 4 for conventional TS diagnostics at three scattering angles. Although circular incident polarization yields stronger depolarization of scattered radiation, rigorous minimization of the error bars shows that linear incident polarization is preferential for polarization-based diagnostics.

III. INTERFEROMETRY AND POLARIMETRY

The ITER TIP system is designed for line-integrated tangential plasma density measurement from both traditional interferometry and Faraday-effect polarimetry.[3] Faraday-effect polarimetry can be used to independently measure the plasma density, since the toroidal magnetic field is known, or to correct the interferometer for fringe jumps. In a cold plasma, the interferometric phase Φ and the Faraday rotation angle of polarization ψ_F are proportional to the line integral of the electron density and the line integral of the electron density multiplied by the parallel component of the magnetic

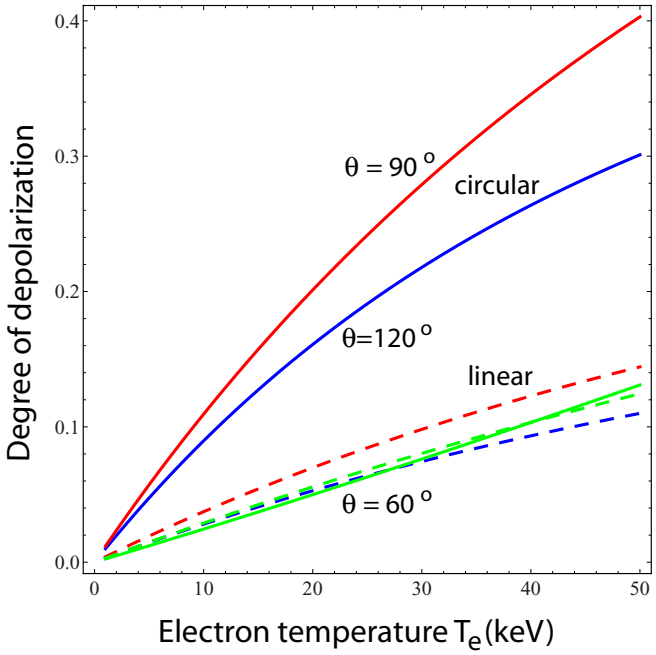

FIG. 4. Depolarization degree vs T_e for three scattering angles: 60° (green), 90° (red), and 120° (blue) (solid lines: circular polarization at $\chi = 45°$; dashed lines: linear polarization at $\psi = \chi = 0$).

field, respectively. For the ITER TIP system parameters, $n \simeq 10^{20} m^{-3}$, $B_{\|} \simeq 5.3T$, $L \simeq 21m$, $\lambda = 10.6\mu m$, $\Phi^{(cold)} \simeq 63$ rad, and $\psi_F \simeq 19°$. The ITER PoPola diagnostic is based on Faraday and Cotton-Mouton effects for laser beams launched in the poloidal plane. It will provide a unique method of internal magnetic field and current profile measurement, in addition to electron density.[4] With propagation largely perpendicular to the magnetic field, the Cotton-Mouton effect becomes significant and leads to a change in the ellipticity angle χ. For the PoPola system parameters, $n \simeq 10^{20} m^{-3}$, $B_{\perp} \simeq 5.3T$, $L \simeq 8m$, and $\lambda = 118\mu m$, the induced ellipticity of radiation initially linearly polarized at 45^0 to $\mathbf{B}_{\perp}$ is given by $\chi^{(cold)} \simeq 52°$.

These results for the I/P characteristics are derived from a cold plasma model. One source of error is finite electron temperature effects neglected in the cold plasma dispersion relation. Thermal corrections are proportional to $\tau = T_e/m_e c^2$ and are small at $T_e \sim 1$ keV, but become sizable at $T_e \geq 10$ keV. There are two physically different sources of thermal corrections that are comparable in magnitude but contribute with opposite sign: non-relativistic Doppler-like effects, and the relativistic electron mass dependence on velocity. The effects of finite electron temperature were addressed in the non-relativistic limit in Ref. 11. Our reevaluation of this problem demonstrated that weakly relativistic effects are equally important and cannot be ignored.[2] The relativistic effects turn out to be stronger than the non-relativistic contributions for interferometry and Faraday-effect polarimetry. They change the sign of the non-relativistic corrections for the interferometric phase and Faraday rotation angle, and reduce the magnitude of the non-relativistic thermal correction for the Cotton-Mouton effect. At $T_e = 25$ keV, the resulting values of the interferometry, FR, CM effects relative to their values in cold plasma are, respectively, −7.5%, −10%, and +22.5%, while the non-relativistic model yields overestimated values, +5%, +15%, and +60%, correspondingly.

For formal analysis of the problem, we developed an iterative technique for solving the relativistic Vlasov kinetic equation. The key element of the method is expansion in powers of $Y = \omega_{ce}/\omega \ll 1$ instead of integration over azimuthal angle in the velocity space. This avoids the use of a complicated Bessel function series representation. Instead, expansion is performed by successive differentiations of simple standard trigonometric functions. The final result is in the analytic form of a double power series expansion of the dielectric tensor in $Y \ll 1$ and $\tau \ll 1$ to any desirable order. The validity of the method has been proven computationally by comparison with the ray-tracing numerical code GENRAY of Ref. 12. The theoretical predictions have also been confirmed by direct measurements on the JET tokamak.[13] Data collected from high-T_e JET discharges demonstrated good agreement with the relativistic theory and disagreement with the cold plasma and non-relativistic models. These were the first experimental observations of relativistic effects in plasma polarimetry.

The model which adequately describes evolution of polarization of the EM wave in a nonuniform plasma and magnetic field is based on the Stokes vector equation[14]

$$\frac{d\mathbf{s}}{dz} = \Omega \times \mathbf{s},$$

where the three-component unit Stokes vector $\mathbf{s}$ is defined in Sec. II, z is a coordinate along the propagation direction and the spatially varying angular velocity vector $\mathbf{\Omega}(z)$ depends on plasma and magnetic field parameters. The Ω_1 and Ω_2 components are responsible for the CM effect and Ω_3 describes the Faraday rotation. This equation takes into account coupling between FR and CM effects due to the quasi-perpendicular directions of the optical paths in ITER PoPola system. The Stokes vector equation allows us to address the issue of the coupling while properly accounting for the thermal effects. Linear in τ temperature corrections were incorporated in this model in Ref. 2. The precision of this lowest-order linear in τ model may be insufficient; using the same iterative technique we recently constructed a more sophisticated model[15] with τ^2-order corrections to satisfy the accuracy requirements for the ITER TIP and PoPola systems. The corresponding expression for Ω is presented in Ref. 15. We illustrate here the structure of linear and τ^2 corrections by using the interferometric phase Φ as an example. Relative deviation of Φ from its cold plasma value $\Phi^{(cold)}$ is caused by the thermal effects and reads

$$\frac{\Delta\Phi^{(T)}}{\Phi^{(cold)}} = \left(-\frac{3}{2}\int \frac{n_e T_e}{m_e c^2} dz + \frac{15}{8}\int \frac{n_e T_e^2}{m_e^2 c^4} dz\right) \Big/ \int n_e dz.$$

For the ITER TIP system with a CO_2 laser at $\lambda = 10.6\mu$m, a central viewing channel optical path length of 21 m, a plasma density of $10^{20} m^{-3}$, and $T_e = 25$ keV, the linear thermal correction to the interferometric phase is large (∼270°), and the quadratic correction is also significant (∼17°). With the τ^2-model and T_e known from Thomson scattering, finite T_e

effects can be rapidly and accurately calculated. This capability is particularly important for fast real-time feedback corrections in ITER.

New effects come into play when the electron distribution function develops an anisotropy. This could be caused by a large mean electron drift velocity $U_{\|e}$ (parallel equilibrium current), an enhanced effective perpendicular temperature $T_\perp$ in ECRH heated plasmas, or a large effective parallel temperature $T_\|$ due to LH current drive. The corresponding vector $\mathbf{\Omega}$ in the Stokes equation can be presented as a sum of three contributions $\mathbf{\Omega} = \mathbf{\Omega}^{(0)} + \mathbf{\Omega}^{(B)} + \mathbf{\Omega}^{(U)}$. The first term does not depend on the magnetic field and describes the effect of birefringence caused by the temperature anisotropy

$$\Omega^{(0)} = (1 - N^2)\frac{\omega X}{2c}\frac{(T_\| - T_\perp)}{m_e c^2}\begin{pmatrix}1\\1\\0\end{pmatrix} \propto \frac{\omega X^2}{2c}\frac{(T_\| - T_\perp)}{m_e c^2}$$

where $X = \omega_{pe}^2/\omega^2$. It results in evolution of the polarization ellipse similar to the usual "magnetic" Cotton-Mouton effect. The magnitude of the effect is strongly reduced by almost exact cancellation of the relativistic and non-relativistic Doppler-like contributions expressed, correspondingly, by the unity and N^2 term in the factor $(1 - N)^2 \propto X$. The residual small effect ($\propto X^2$) exceeds "magnetic" Cotton-Mouton effect in high-β plasmas. In the low-β case, it can be a potential source of $1\% - 3\%$ errors for the ITER PoPola diagnostic system.

The second term, $\mathbf{\Omega}^{(B)}$, describes the generalization of linear in τ isotropic results to the case of non-Maxwellian anisotropic distributions. These results can be used for correction of the interpretation errors in fusion plasmas with non-Maxwellian distributions generated by ECRH and other RF sources such as EC and LH current drive

$$\Omega^{(B)} = \Omega^{(c)} + \cos 2\alpha \frac{(T_\| - T_\perp)}{2m_e c^2}\begin{pmatrix}10\Omega_1^{(c)}\\10\Omega_2^{(c)}\\3\Omega_3^{(c)}\end{pmatrix} + \frac{1}{2m_e c^2}$$

$$\times \begin{pmatrix}(5T_\| + 4T_\perp)\Omega_1^{(c)}\\(5T_\| + 4T_\perp)\Omega_2^{(c)}\\-(3T_\| + T_\perp)\Omega_3^{(c)}\end{pmatrix}, \Omega^{(c)} = \frac{\omega}{2c}\begin{pmatrix}XY^2 \sin^2\alpha \cos 2\beta\\XY^2 \sin^2\alpha \sin 2\beta\\2XY \cos\alpha\end{pmatrix},$$

where α and β are spatially varying angles of the magnetic field $\mathbf{B}$ in a spherical reference frame with $\mathbf{z}\|\mathbf{k}$ (α is the angle between $\mathbf{k}$ and $\mathbf{B}$ and β is the azimuth angle in the x, y plane between $\mathbf{x}$ and $\mathbf{B}_\perp$).

Motion of the electron component as a whole (equilibrium current) can be treated in terms of the Fizeau effect, that is, the phase velocity of electromagnetic waves depends on whether they propagate in a moving or stationary medium. This suggests a new interferometric scheme for measuring the equilibrium current density by comparing the phases of two counter-propagating laser beams. This method was proposed to measure the line integrated poloidal electron current.[16] Lorentz-transformation based calculations for a plasma slab moving with velocity U_e orthogonal to the slab boundary predicted a measurable interferometric phase shift $\Delta\phi \simeq (\omega/c)(U_e/c)XL \simeq 2^\circ$ with a FIR laser at $\lambda = 432\mu$m, a central viewing optical path length of 1 m, a plasma density of $1.5 \times 10^{19} m^{-3}$, and current density $\sim$1.5 MA/m^2. A more sophisticated slab model with the velocity vector oriented arbitrarily with respect to the slab surface showed that in a cold non-magnetized plasma, only the velocity component perpendicular to the plasma density isosurface can be measured.[17] For the parallel component, which is of the main interest for current density diagnostics, the Fizeau effect cancels out due to specific scaling of plasma refractive index on frequency.[18] This can also be seen from the structure of the isotropic electron dielectric tensor which is insensitive to the Doppler shift of the frequency $\mathbf{k} \cdot \mathbf{U}$ caused by the mean electron velocity.

In the presence of a magnetic field, the non-magnetized electron dispersion relation is modified. Calculating the electron dielectric tensor, we found new physical properties of the Fizeau effect. They appear in the form of birefringence of electromagnetic waves due to the combined action of the magnetic field and electron drift velocity. The Fizeau effect is recovered in a magnetized plasma because the Dopper shifted frequencies do not cancel in magnetic field dependent elements of the dielectric tensor. Evolution of the wave polarization caused by parallel electron equilibrium current is described by the Stokes vector equation with the vector $\mathbf{\Omega}^{(U)}$

$$\Omega^{(U)} = \frac{\omega U_{\|e}}{c^2}\begin{pmatrix}XY^2 \cos\alpha \sin^2\alpha \cos 2\beta\\XY^2 \cos\alpha \sin^2\alpha \sin 2\beta\\XY \cos 2\alpha\end{pmatrix}.$$

This may open new possibilities for diagnosis or measurements of the parallel equilibrium current (Fizeau polarimetry).[19]

IV. SUMMARY

Using the theoretical model for TS polarization allows us to optimize the experimental setup for polarization-based T_e measurements. For optimization, the diagnostic error bars are calculated and minimized with respect to polarization characteristics of the incident light ψ and χ and scattering angle θ. In the general case of elliptically polarized incident light, four Stokes vector components of the scattered light should be measured. Modifying the standard scheme of six measurable intensities,[10] we select four independent intensities I_α to determine $\mathbf{S}^{(s)}$

$$S_0^{(s)} = I_{0^\circ} + I_{90^\circ}, S_1^{(s)} = I_{0^\circ} - I_{90^\circ},$$
$$S_2^{(s)} = I_{0^\circ} + I_{90^\circ} - 2I_{135^\circ}, S_3^{(s)} = I_{0^\circ} + I_{90^\circ} - 2I_{135^\circ}^{\pi/2}.$$

Three of them are measured after the light is separated by beamsplitters and transmitted by three polarizers that select linear polarization at the azimuth angles 0°, 90°, and 135° with respect to the perpendicular to the scattering plane. The fourth channel contains a quater-wave plate to create $\pi/2$ retardation of the in-plane component before the light is transmitted by the 135° polarizer. The degree of depolarization measurement error, σ_D, is related to the error on each of the

statistically independent intensity measurements σ_{I_α}

$$\sigma_D^2 = \sum_\alpha \left(\frac{\partial D}{\partial I_\alpha}\right)^2 \sigma_{I_\alpha}^2,$$

where the intensity measurement errors are determined by Poisson statistics such that $\sigma_{I_\alpha}^2 \propto I_\alpha$. The relative error in the electron temperature measurement, $\sigma_{T_e}/T_e = \sigma_D(T_e \partial D/\partial T_e)^{-1} = W/(\sqrt{Q} T_e \partial D/\partial T_e)$, is presented by a product of two universal functions $W(\psi, \chi, \theta, T_e)$ and $(\partial D/\partial T_e)^{-1}(\psi, \chi, \theta, T_e)$ with a scaling factor $1/\sqrt{Q}$ which does not depend on the polarization variables (Q is effectively proportional to the total number of scattered photons). The factorization allows us to perform minimization of σ_{T_e} analytically for the full range of incident polarizations, scattering angles, and electron temperatures. Although Fig. 4 shows that at $\theta = 90^\circ$ and $\theta = 120^\circ$, the derivative $\partial D/\partial T_e$ is the largest for circular polarization, fast growth of W in this parameter range determines the overall minimum of the error bars at linear incident polarization with $\chi = \psi = 0$. This proves that the regime of linear polarization with $\psi = 0$ is optimal not only because of the convenience of two-channel measurements but due to intrinsic polarization properties of Thomson scattered radiation. More detailed analysis is presented in Ref. 20. At $\theta \sim 90^\circ$ and $T_e > 9$ keV, the error bars are less than 5%, and less than 2% above 23 keV making polarization-based diagnostics competitive with standard spectrum-based measurements.

For ITER polarimetry (FR and CM) and interferometry measurements, it is proposed to use retroreflection of the I/P probing laser beams so that the beam enters and exits through the same port. With retroreflection, the FR and CM effects on the input and return paths are additive if the retroreflection is performed through an odd number of reflections and subtractive if the number of reflections is even.[21] Evolution of polarization resulting from the mean electron velocity and described by $\mathbf{\Omega}^{(U)}$ exhibits an opposite response and is additive in the case of an even number of reflections. If polarization effects are small enough, using the roof-top reflector (RTR) allows us to eliminate contributions from magnetic FR and CM effects described by the $\mathbf{\Omega}^{(B)}$ vector and detect the signal determined by the pure $\mathbf{\Omega}^{(U)}$ effect. Using FIR laser wavelength $\lambda = 432\mu$m with parallel propagation ($\alpha = 0$) along the central viewing cord of ITER TIP system and double-passed retro-reflection from RTR, yields the angle of rotation of polarization $\psi_U \sim 15^\circ$ at $U_{\|e}/c \sim 5 \times 10^{-4}$. Another effect is predicted in the case of quasi-perpendicular propagation $\alpha = 90^\circ$. Then, the magnetic Faraday effect cancels out while rotation of the polarization plane still takes place due to birefringence described by $\Omega_3^{(U)}$ term with $\cos 2\alpha = -1$.

ACKNOWLEDGMENTS

This material is based on work supported by the U.S. Department of Energy Office of Science, Office of Fusion Energy Sciences under Award Nos. DE-FC02-05ER54814, DE-FG02-01ER54615, the U.S. NSF Cooperative Agreement No. PHY-0821899 Center for Magnetic Self-Organization in Laboratory and Astrophysical Plasmas and the U.S. ITER Project Office.

[1] I. H. Hutchinson, *Principles of Plasma Diagnostics* (Cambridge University Press, 2002), p. 440.
[2] V. V. Mirnov, W. X. Ding, D. L. Brower, M. A. Van Zeeland, and T. N. Carlstrom, Phys. Plasmas **14**, 102105 (2007).
[3] M. A. Van Zeeland, R. L. Boivin, D. L. Brower, T. N. Carlstrom, J. A. Chavez, W. X. Ding, R. Feder, D. Johnson, L. Lin, R. C. O'Neill, and C. Watts, Rev. Sci. Instrum. **84**, 043501 (2013).
[4] R. Imazawa, Y. Kawano, and Y. Kusama, Nucl. Fusion **51**, 113022 (2011).
[5] F. Orsitto and N. Tartoni, Rev. Sci. Instrum. **70**, 798 (1999).
[6] J. Sheffield, D. H. Froula, S. H. Glenzer, and N. C. Luhmann, *Plasma Scattering of Electromagnetic Radiation*, 2nd ed. (Academic Press, 2011), p. 520.
[7] S. E. Segre and V. Zanza, Phys. Plasmas **7**, 2677 (2000).
[8] R. E. Pechacek and A. W. Trivelpiece, Phys. Fluids **10**, 1688 (1967).
[9] V. V. Mirnov, D. L. Brower, D. J. Den Hartog, W. X. Ding, J. Duff, and E. Parke, *Proceedings of 24th International Conference on Fusion Energy*, ITR/P5-32, San Diego, CA (IAEA, Vienna, 2012).
[10] M. Born and E. Wolf, *Principles of Optics*, 3nd ed. (Pergamon Press, 1965), p. 808.
[11] S. E. Segre and V. Zanza, Phys. Plasmas **9**, 2919 (2002).
[12] A. P. Smirnov, R. W. Harvey, and K. Kupfer, Bull. Am. Phys. Soc. **39**, 1626 (1994).
[13] O. P. Ford, J. Svensson, A. Boboc, D. C. McDonald, and JET EFDA Contributors, Plasma Phys. Controlled Fusion **51**, 065004 (2009).
[14] S. E. Segre, Plasma Phys. Controlled Fusion **41**, R57 (1999).
[15] V. V. Mirnov, D. L. Brower, D. J. Den Hartog, W. X. Ding, J. Duff, and E. Parke, Nucl. Fusion **53**, 113005 (2013).
[16] D. L. Brower, W. X. Ding, B. H. Deng, M. A. Mahdavi, V. Mirnov, and S. C. Prager, Rev. Sci. Instrum. **75**, 3399 (2004).
[17] V. V. Mirnov, D. L. Brower, and W. X. Ding, *Collection of Abstracts of International Sherwood Fusion Energy Conference*, Boulder, CO (2008) (http://sherwood.colorado.edu/Uploads/MIRNOV__onpossib3101_10.pdf).
[18] I. Lerche, Am. J. Phys. **43**, 910 (1975).
[19] V. V. Mirnov, D. L. Brower, D. J. Den Hartog, W. X. Ding, J. Duff, and E. Parke, submitted to *AIP Proceedings of International Conference on Fusion Reactor Diagnostics*, Varenna, Italy (AIP Publishing, 2014), vol. 1609.
[20] E. Parke, V. V. Mirnov, and D. J. Den Hartog, *Proceedings of the 16th International Symposium on Laser-Aided Plasma Diagnostics* (Madison, WI, 2013) ; J. Instrum. **9**, C02030 (2014).
[21] S. E. Segre and V. Zanza, Plasma Phys. Controlled Fusion **50**, 105006 (2008).